

Lattice gauge theories and string dynamics in Rydberg atom quantum simulators

Federica M. Surace,^{1,2} Paolo P. Mazza,^{1,3} Giuliano Giudici,^{1,3}
Alessio Lerose,^{1,3} Andrea Gambassi,^{1,3} and Marcello Dalmonte^{1,2}

¹*SISSA – International School for Advanced Studies, via Bonomea 265, 34136 Trieste, Italy.*

²*ICTP – International Center for Theoretical Physics, Strada Costiera 11, 34151 Trieste, Italy.*

³*INFN, Sezione di Trieste, via Bonomea 265, 34136 Trieste, Italy.*

Gauge theories are the cornerstone of our understanding of fundamental interactions among particles. Their properties are often probed in dynamical experiments, such as those performed at ion colliders and high-intensity laser facilities. Describing the evolution of these strongly coupled systems is a formidable challenge for classical computers, and represents one of the key open quests for quantum simulation approaches to particle physics phenomena. Here, we show how recent experiments done on Rydberg atom chains naturally realize the real-time dynamics of a lattice gauge theory at system sizes at the boundary of classical computational methods. We prove that the constrained Hamiltonian dynamics induced by strong Rydberg interactions maps exactly onto the one of a $U(1)$ lattice gauge theory. Building on this correspondence, we show that the recently observed anomalously slow dynamics corresponds to a string-inversion mechanism, reminiscent of the string-breaking typically observed in gauge theories. This underlies the generality of this slow dynamics, which we illustrate in the context of one-dimensional quantum electrodynamics on the lattice. Within the same platform, we propose a set of experiments that generically show long-lived oscillations, including the evolution of particle-antiparticle pairs. Our work shows that the state of the art for quantum simulation of lattice gauge theories is at 51 qubits, and connects the recently observed slow dynamics in atomic systems to archetypal phenomena in particle physics.

Introduction

Lattice gauge theories (LGTs) [1] represent one of the most successful framework for describing fundamental interactions within the standard model of particle physics. Numerical simulations of their Euclidean formulation [2] have shed light on paradigmatic equilibrium properties of strong interactions, including the low-lying spectrum of quantum chromodynamics [3], and the nature of its phase diagram [4, 5]. Non-equilibrium properties, instead, are a notable challenge [6], due to the lack of generically applicable methods to simulate the real-time dynamics of extended, strongly interacting systems [7]. This has stimulated an intense theoretical activity aimed at quantum simulating LGTs via atomic quantum systems [8–10], leading to the first door-opener experimental realization in a system of four trapped ions [11]. While such quantum simulators have already challenged the most advanced computational techniques in regard of condensed-matter motivated models [12, 13], there is presently no experimental evidence that atomic systems can be used to simulate LGTs at large scales, nor that they can display physical phenomena with a direct counterpart in LGTs. This limitation stems from the very characteristic aspect that distinguishes LGTs from other statistical mechanics models, i.e. the presence of local constraints on the possible configurations, in the form of a Gauss law, which cannot be easily implemented in actual experimental realizations [8, 9].

Here, we show that (1+1)-dimensional LGTs akin to quantum electrodynamics are naturally realized in state-of-the-art experiments with Rydberg atom arrays [14, 15]. In particular, we show how the dynamics of Rydberg excitations in these chains is exactly mapped onto a spin-1/2 quantum link model (QLM), a $U(1)$ LGT where the gauge fields span a finite-dimensional Hilbert space, equivalent to a lattice Schwinger

model in the presence of a topological term [16]. The key element of our mapping, which is schematically illustrated in Fig. 1, is that gauge invariance has a natural counterpart in the Rydberg blockade mechanism, which constrains the Hilbert space in the same way as Gauss law does in gauge theories. This provides an immediate interpretation of the recent experiment with Rydberg-blockaded atom arrays in Ref. [14] as the first large-scale quantum simulation of a LGT at the edge of classical computational methods [7].

From a theoretical viewpoint, the mapping offers a hitherto unexplored perspective on the anomalously slow relaxation recently observed in experiments: the long-lived oscillations in the population of excited Rydberg atoms correspond to a string inversion, a phenomenon which is directly tied to string breaking [6, 17, 18] prototypical of gauge theories including dynamical matter (cf. Fig. 1d and 1e). The mapping indicates that this phenomenon has a natural interpretation in the LGT framework, and suggests the occurrence of slow dynamics in other $U(1)$ gauge theories, such as higher-spin QLMs [19] and the Schwinger model [20, 21]. These theories have been widely discussed in the context of Schwinger pair production taking place at high-intensity laser facilities, thus providing a highly unexpected, direct link between apparently unrelated experimental platforms [18, 22–25].

We discuss the generality of this type of quantum evolution by extending our analysis to other relevant instances of "slow dynamics", characterized by the absence of relaxation on all time scales corresponding to any microscopic coupling present in the system. As initial states, we focus on those consisting of particle-antiparticle pairs, corresponding to regular configurations of the Rydberg-atom arrays with localized defects, which are accessible within the setup of Ref. [14]. We show that these defects propagate ballistically with long-lived coherent interference patterns. This behavior is found

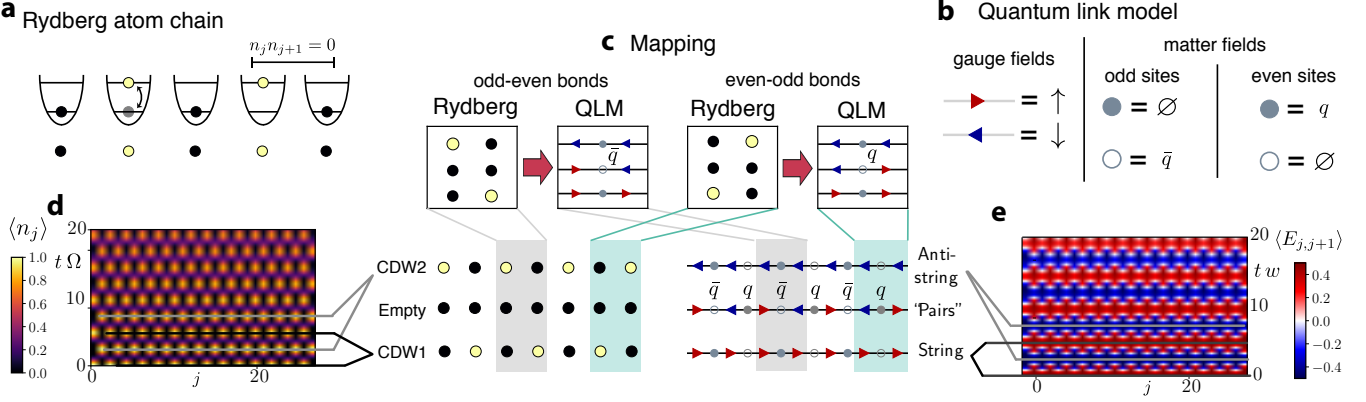


Figure 1: Gauge-theory interpretation of Rydberg-atom quantum simulations. **a:** Schematics of a Rydberg atom chain. Each potential well of the optical lattice hosts a single atom, which can be either in the ground (black) or excited Rydberg (yellow) state. The two levels are coupled by a laser field. The Rydberg blockade prevents the simultaneous excitations of neighboring atoms. **b:** Degrees of freedom of a $U(1)$ LGT in the spin-1/2 quantum link model (QLM) formulation. Gauge fields are represented by spin variables residing on links. Matter fields are represented by Kogut-Susskind fermions: an occupied site corresponds to the vacuum on odd sites, and to a quark q on even sites. An empty site, instead, to the vacuum on even sites and to an anti-quark \bar{q} on odd sites. **c:** Mapping between Rydberg-blockaded states and configurations of the electric field constrained by the Gauss law in the QLM. Due to the staggered electric charge, the allowed configurations of the electric field depend on the link, as illustrated. The two so-called charge-density wave configurations “CDW1” and “CDW2” of the Rydberg-atom arrays are mapped onto the “string” and “anti-string” states, respectively, characterized by uniform rightward or leftward electric fluxes. The empty configuration with all Rydberg atoms in their ground state is mapped to a state filled by adjacent particle-antiparticle pairs. **d:** Time evolution starting from the CDW1 state. The plot shows the space and time resolved population $\langle n_j \rangle$ of the excited Rydberg atoms. **e:** Evolution of the expectation value of the electric field operator $\hat{E}_{j,j+1}$ in the QLM. These dynamics maps exactly onto the ones shown in panel **d** via the mapping illustrated in panel **c**. The thin lines highlight the oscillation between CDW1, CDW2 (left, bottom of panel **c**) or string and anti-string (right) states. In these simulations, $L = 24$ and $U = m = 0$.

to be governed by special bands of highly excited eigenstates characterized by a regularity in the energy-momentum dispersion relation. These findings open up a novel perspective which complements and extends towards gauge theories recent approaches to slow relaxation in Rydberg-blockaded atomic chains [26–31].

Rydberg atom arrays

We are interested here in the dynamics of a one-dimensional array of L optical traps, each of them hosting a single atom, as schematically illustrated in Fig. 1a. The atoms are trapped in their electronic ground state (black circle), denoted by $|\downarrow\rangle_j$, where j numbers the trap. These ground states are quasi-resonantly coupled to a single Rydberg state, i.e., a highly excited electronic level, denoted by $|\uparrow\rangle_j$. The dynamics of this chain of qubits $\{|\uparrow, \downarrow\rangle_j\}_{j=1, \dots, L}$ is governed by the following Ising-type Hamiltonian [13, 32]:

$$\hat{H}_{\text{Ryd}} = \sum_{j=1}^L (\Omega \hat{\sigma}_j^x + \delta \hat{\sigma}_j^z) + \sum_{j \neq \ell=1}^L V_{j,\ell} (\hat{\sigma}_j^z + 1)(\hat{\sigma}_\ell^z + 1), \quad (1)$$

where Ω and δ are the Rabi frequency and the detuning of the laser excitation scheme, respectively, $V_{j,\ell}$ describes the interactions between atoms in their Rydberg states at sites (j, ℓ) , and $\hat{\sigma}_j^\alpha$ are Pauli matrices at site j . For the cases of interest here, this interaction is strong at short distances and decays

as $1/|j - \ell|^6$ at large distances. The dynamics described by \hat{H}_{Ryd} has already been realized in several experiments utilizing either optical lattices or optical tweezers [14, 15, 33]. In particular, Ref. [14] investigated the case in which $V_{j,j+1}$ is much larger than all other energy scales of the system, resulting in the so-called Rydberg blockade effect: atoms on neighboring sites cannot be simultaneously excited to the Rydberg state, hence the constraint $\hat{n}_j \hat{n}_{j+1} = 0$, where the operator $\hat{n}_j = (\hat{\sigma}_j^z + 1)/2$ signals the presence of a Rydberg excitation at site j .

In this regime, the resulting Hamiltonian — introduced by Fendley, Sengupta and Sachdev (FSS) in Ref. [34] — is

$$\hat{H}_{\text{FSS}} = \sum_{j=1}^L (\Omega \hat{\sigma}_j^x + 2\delta \hat{n}_j), \quad (2)$$

where we neglect longer-range terms which do not affect qualitatively the dynamics. \hat{H}_{FSS} acts on the constrained Hilbert space without double occupancies on nearest-neighbor sites, as illustrated in Fig. 1a. As we show below, the direct connection between Rydberg atomic systems and gauge theories is indeed provided by this constraint at the level of the Hilbert space.

Rydberg blockade as a gauge symmetry constraint

We establish here the exact mapping between the FSS Hamiltonian in Eq. (2) governing the dynamics of the Rydberg atom quantum simulator in Ref. [14] and a $U(1)$ LGT. The latter describes the interaction between fermionic particles, denoted by $\hat{\Phi}_j$ and residing on the lattice site j , mediated by a $U(1)$ gauge field, i.e., the electric field $\hat{E}_{j,j+1}$, defined on lattice bonds, as depicted in Fig. 1b. We use here Kogut-Susskind (staggered) fermions [21], with the conventions that holes on odd sites represent antiquarks \bar{q} , while particles on even sites represent quarks q . Their dynamics is described by:

$$\hat{H} = -w \sum_{j=1}^{L-1} (\hat{\Phi}_j^\dagger \hat{U}_{j,j+1} \hat{\Phi}_{j+1} + \text{h.c.}) + m \sum_{j=1}^L (-1)^j \hat{\Phi}_j^\dagger \hat{\Phi}_j + J \sum_{j=1}^{L-1} \hat{E}_{j,j+1}^2, \quad (3)$$

where the first term provides the minimal coupling between gauge and matter fields through the parallel transporter $\hat{U}_{j,j+1}$ with $[\hat{E}_{j,j+1}, \hat{U}_{j,j+1}] = \hat{U}_{j,j+1}$, the second term is the fermion mass, and the last one is the electric field energy. The generators of the $U(1)$ gauge symmetry are defined as

$$\hat{G}_j = \hat{E}_{j,j+1} - \hat{E}_{j-1,j} - \hat{\Phi}_j^\dagger \hat{\Phi}_j + \frac{1 - (-1)^j}{2}, \quad (4)$$

and satisfy $[\hat{H}, \hat{G}_j] = 0$, so that gauge invariant states $|\Psi\rangle$ satisfy Gauss law $\hat{G}_j |\Psi\rangle = 0$ for all values of j . Restricting the dynamics to their subspace is by far the most challenging task for quantum simulators.

Different formulations of $U(1)$ LGTs are obtained for different representations of gauge degrees of freedom $\hat{E}_{j,j+1}$. While in the standard Wilsonian formulation — i.e., the lattice Schwinger model — they span infinite-dimensional Hilbert spaces, here we first focus on the $U(1)$ QLM formulation [35, 36], where they are represented by spin variables, i.e., $\hat{E}_{j,j+1} = \hat{S}_{j,j+1}^z$ and $\hat{U}_{j,j+1} = \hat{S}_{j,j+1}^+$, so that $[\hat{E}_{j,j+1}, \hat{S}_{j,j+1}^+] = \hat{S}_{j,j+1}^+$. As noted in Ref. [37], this formulation is particularly suited for quantum simulation purposes.

In the following, we consider the QLM with spin $S = 1/2$, in which all the possible configurations of the electric field have the same electrostatic energy, rendering the value of J inconsequential; we anticipate that this model is equivalent to the lattice Schwinger model in the presence of a θ -angle with $\theta = \pi$. The Hilbert space structure following Gauss law is particularly simple in this case [37]: as depicted in Fig. 1c, for each block along the chain consisting of two electric fields neighbouring a matter field at site j , there are only three possible states, depending on the parity of j . In fact, in a general (1+1)-dimensional $U(1)$ LGT, the configuration of the electric field along the chain determines the configuration of the charges via the Gauss law. Accordingly, \hat{H} in Eq. (3) can be recast into a form in which the matter fields $\hat{\Phi}_j$ are integrated out.

We now provide a transformation which maps exactly the latter form into the FSS Hamiltonian (2). The correspondence between the two Hilbert spaces is realized by identifying, alternately on odd and even lattice sites, the computational basis configurations of the atomic qubits allowed by the Rydberg blockade with the classical configurations of the electric field allowed by the Gauss law (see Fig. 1c). In terms of the two Hamiltonians (2) and (3), this unitary transformation consists in identifying the operators $\hat{\sigma}_j^x \leftrightarrow 2\hat{S}_{j-1,j}^x$, $\hat{\sigma}_j^{y,z} \leftrightarrow (-1)^j 2\hat{S}_{j-1,j}^{y,z}$ and the parameters $\Omega = -w$, $\delta = -m$. This mapping overcomes the most challenging task in quantum simulating gauge theories, by restricting the dynamics directly within the gauge-invariant Hilbert space. The only states that would violate Gauss law are nearest-neighbor occupied sites which are strongly suppressed by the Rydberg blockade and can be systematically excluded via post-selection of the configurations. Beyond providing a direct link between Gauss law and the Rydberg blockade mechanism, the most important feature of the mapping is that, differently from other remarkable relations between \hat{H}_{FSS} and lattice models with gauge symmetries [38, 39], it provides an immediate connections between Rydberg experiments and particle physics phenomena, as we describe below.

Gauge-theory interpretation of slow dynamics

The exact description of Rydberg-blockaded chains in terms of a $U(1)$ LGT allows us to shed a new light on the slow dynamics reported in Ref. [14], by interpreting them in terms of well-studied phenomena in high-energy physics, related to the production of particle-antiparticle pairs after a quench akin to the Schwinger mechanism.

In the experiment, the system was initialized in a charge density wave state (CDW1 in Fig. 1c), and subsequently, the Hamiltonian was quenched, inducing slowly-decaying oscillations between CDW1 and CDW2. As shown in Fig. 1c, CDW1 and CDW2 are mapped onto the two states of the $S = 1/2$ -QLM with uniform electric field $\hat{S}_{j,j+1}^z = \pm 1/2$. The experimental results in Ref. [14] may thus be interpreted as the evolution starting from one of the two degenerate bare particle vacua $|0_{\pm}\rangle$ (i.e, the vacua in the absence of quantum fluctuations, $w = 0$) of the gauge theory. In Fig. 1d and in the first column of Fig. 2, we illustrate these dynamics as it would be observed in the excitation density $\langle n_j \rangle$ along the Rydberg-atom quantum simulators ("Rydberg") and compare it with that of the electric field $\langle E_{j,j+1} \rangle$ within its gauge-theory description ("QLM") in Fig. 1e and in the second column of Fig. 2, respectively, utilizing exact diagonalization.

The qualitative features of this evolution are strongly affected by quantum fluctuations, whose impact is quantified by the ratio between the coupling constant w and the particles mass m . For small values of m/w (first two lines in Fig. 2), production of particle-antiparticle pairs occurs at a finite rate. We remark that this effect is reminiscent of the

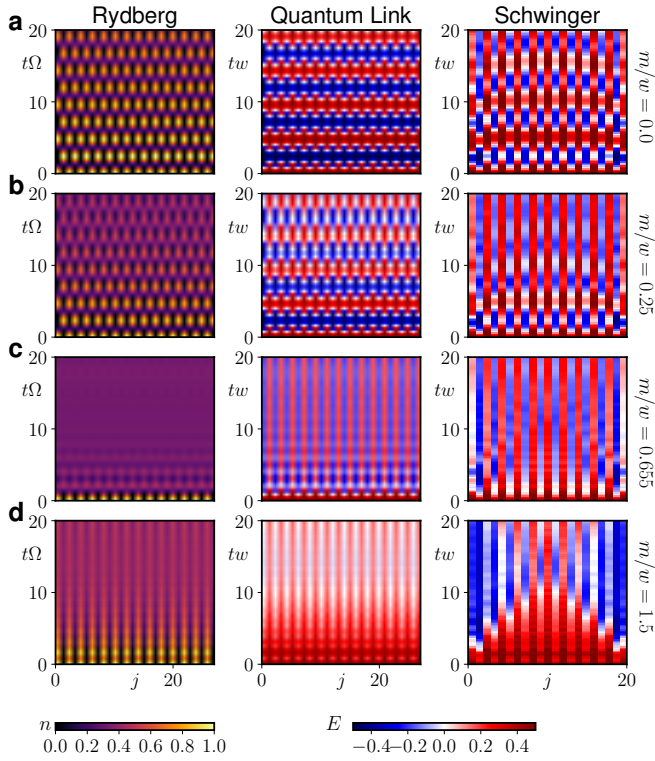


Figure 2: Slow dynamics in Rydberg atoms, $U(1)$ quantum link model (QLM), and the lattice Schwinger model. Coherent quantum evolution of (first column) the local Rydberg excitation density profile $n_j(t) = \langle \hat{n}_j(t) \rangle$ in the FSS model [see Eq. (2)], starting from a charge-density wave, of the local electric field profile (second column) $E_{j,j+1}(t) = \langle \hat{S}_{j,j+1}^z(t) \rangle$ in the QLM, and (third column) $\langle \hat{L}_{j,j+1}(t) - \theta/(2\pi) \rangle$ (see further below in the main text) in the lattice Schwinger model [see Eq. (3)] with $J/w = 1.5$ and $\theta = \pi$. The four rows correspond to increasing values of the detuning δ (Rydberg) or, equivalently, of the particles mass $m = -\delta$ (QLM and Schwinger model). Figures 1d and 1e correspond to the first two plots in panel **a** here. Data in the first and second columns are connected by a unitary transformation, while a remarkable similarity is manifest between the second and third column despite the larger Hilbert space of the gauge degrees of freedom in the Schwinger model. The persistent string inversions observed within the symmetric phase with $m < m_c = 0.655|w|$ (first two lines) are suppressed as the quantum critical point is approached. The dynamics in panels **c** and **d** of the third column features edge effects due to the imposed open boundary conditions.

Schwinger mechanism [6], which however concerns pair creation from the true (and not the bare) vacuum. These particles get accelerated by the electric field and progressively screen it, until coherent pair annihilation takes place and eventually brings the system to a state with opposite electric flux. This process, referred to as *string inversion*, occurs several times in a coherent fashion, causing a dramatic slowdown of thermalization and of quantum information scrambling. As a further evidence, we compute both the total electric flux and the vacuum return probability (or Loschmidt echo), defined as $G_+(t) = |\langle 0_+ | e^{-i\hat{H}t} | 0_+ \rangle|^2$, whose large value $\simeq 1$

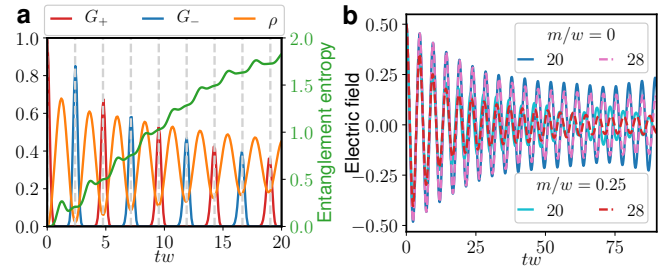


Figure 3: Characterization of slow dynamics in the FSS model. **a:** Hilbert space characterization of the persistent string inversions ($m = 0$, $L = 28$): alternating strong revivals of the overlaps $G_{\pm}(t) = |\langle 0_{\pm} | e^{-i\hat{H}t} | 0_{\pm} \rangle|^2$ with the two bare vacuum states $|0_{\pm}\rangle$, corresponding to the two charge-density wave configurations of Rydberg-atom arrays. Both the total density $\rho = \langle \hat{\rho}_j \rangle$ of particle-antiparticle pairs, with $\hat{\rho}_j = (-1)^j \hat{\Phi}_j^\dagger \hat{\Phi}_j + [1 - (-1)^j]/2$ and the half-chain entanglement entropy (see the supplementary information) have regularly-spaced maxima between the peaks. **b:** Persistent oscillations of electric field for two values of the mass and of the system size.

was already noted in Ref. [40]. The anomalous long-lived oscillations of these quantities experimentally detected with Rydberg atom arrays in Ref. [14] show a clear analogy with several previous numerical studies of the real-time dynamics of higher-spin QLMs [24] as well as of the Schwinger model [22, 23, 41]. In addition, as noted in Ref. [37], the dynamics discussed here describes the coherent oscillations of the parity-symmetric order parameter (in our case, $\langle \hat{E}_{j,j+1} \rangle$) as a function of time, reminiscent of the decay of a chiral condensate in QCD [25]. We thus provide here a bridge among all these observations.

However, if fermionic particles are sufficiently heavy, with m/w exceeding a critical threshold, pair production is a virtual process and string inversion cannot be triggered, as shown in the third and fourth line of Fig. 2. We find that this behavior is related to the quantum phase transition occurring in the FSS model at $\delta_c = -0.655|\Omega|$ [34]. This transition corresponds to the spontaneous breaking of the chiral symmetry in the LGT (4) at $m_c = 0.655|w|$ [42]. The four rows in Fig. 2 show the temporal evolution of the same initial uniform flux configuration (CDW or “string” in Fig. 1c) upon increasing values of the mass $m/w = 0, 0.25, 0.655, 1.5$ corresponding to the dynamics (**a**, **b**) at $m < m_c$, (**c**) at the quantum critical point $m = m_c$, and (**d**) at $m > m_c$.

Figure 3 further illustrates the appearance of string inversions for $m < m_c$ and the corresponding slow dynamics. Panel **a** shows the long-lived revivals of the many-body wavefunction in terms of the evolution of the probability $G_{\pm}(t)$ of finding the system at time t in the initial bare vacuum state $|0_+\rangle$ or in the opposite one $|0_-\rangle$, corresponding to G_+ or G_- , respectively, as well as in terms of the time-dependent density ρ of particle-antiparticle pairs. The entanglement entropy of half system also displays an oscillatory behavior (see supplementary information). Panel **b** shows the scaling of the collective oscillations of the electric field with respect to the

system size L , as well as their persistence with a small but non-vanishing fermion mass $m < m_c$.

Slow dynamics in the lattice Schwinger model

The above phenomenology is not restricted to QLMs, but is expected to be a generic feature of LGTs including dynamical matter. We show this in the context of a Wilsonian LGT, i.e., the lattice version of the Schwinger model in Eq. (3). In this case, $\hat{U}_{j,j+1} = e^{i\hat{\vartheta}_{j,j+1}}$ are $U(1)$ parallel transporters with vector potential $\hat{\vartheta}_{j,j+1}$, the corresponding electric field operator is $\hat{E}_{j,j+1} = \hat{L}_{j,j+1} - \theta/(2\pi)$, where $\hat{L}_{j,j+1}$ have integer spectrum and $\theta/(2\pi)$ represents a uniform classical background field parameterized by the θ -angle. Canonical commutation relations for the gauge degrees of freedom read $[\hat{\vartheta}_{j,j+1}, \hat{L}_{p,p+1}] = i\delta_{jp}$. In our numerical simulations, we utilize the spin formulation of the model obtained upon integration of the gauge fields under open boundary conditions [43, 44].

We consider the case of a θ -angle with $\theta = \pi$, such that two uniform field configurations have equal electrostatic energy. In the limit $J/w \rightarrow \infty$, the lattice Schwinger model is equivalent to the spin-1/2 QLM discussed above. We find evidence that the corresponding behaviour persists qualitatively down to $J \simeq w$, when the electrostatic energy competes with the matter-field interaction, as shown in the third column of Fig. 2. Despite the strong quantum fluctuations allowed in principle by the exploration of a locally infinite-dimensional Hilbert space, a qualitative similarity — which becomes a quantitative correspondence concerning the relationship between the coupling and the period of oscillation — with the case of the locally finite-dimensional Hilbert space of the QLM is manifest in the second column of Fig. 2, related to the observed dynamics in Ref. [14].

In order to highlight the generality of the phenomenology outlined above, we point out here an analogy with the dynamics of the Schwinger model in the continuum limit. In the massless case $m = 0$, the latter is mapped by bosonization to a free scalar bosonic field theory, described by the integrable Hamiltonian in terms of the canonically conjugate fields $\hat{\Pi}$ and $\hat{\phi}$ [6],

$$\hat{H}_B = \int dx \left[\frac{1}{2} \hat{\Pi}^2 + \frac{1}{2} (\partial_x \hat{\phi})^2 + \frac{1}{2} \frac{e^2}{\pi} \hat{\phi}^2 \right]. \quad (5)$$

Within this simplified description, the evolution starting from a false vacuum with $\langle \hat{\phi}(x, t=0) \rangle = \text{const} \neq 0$ will thus show uniform persistent oscillations with a frequency $\omega_0 = e/\sqrt{\pi}$, where e is the charge of the fermion. A non-vanishing m leads to the additional potential term $-cm\omega_0 \cos(2\sqrt{\pi}\hat{\phi} - \theta)$ in the integrand in Eq. (5), such that the resulting total potential shows a transition from a shape with a single minimum for $m < m_c$ to two symmetric minima for $m > m_c$, analogous to the spontaneous breaking of chiral symmetry on the lattice (see the supplementary information for details). For

small m , the integrability of the model is weakly broken and the evolution from a false vacuum features long-lived oscillations, reminiscent of the slow dynamics reported here for the lattice versions of this gauge theory.

Propagation of particle-antiparticle pairs and non-thermal states

States of the QLM corresponding to particle-antiparticle pairs in the bare vacuum can be constructed in Rydberg-atom quantum simulators by preparing two or more defects in a charge-density wave configuration, each corresponding to pairs of adjacent non-excited Rydberg atoms.

As an illustration, we discuss how the time-evolution of one or two particle-antiparticle pairs for $m < m_c$ features the emergence of slow dynamics. In Fig. 4, we show the time evolution of both the particle density in the QLM and the corresponding density of excitations in the Rydberg chain. The pairs in the initial state break and ballistic spreading of quark and antiquark takes place. The string inversion dynamics induced by this propagation shows coherent interference patterns with long-lived oscillations. Due to retardation effects induced by the constrained dynamics, these oscillations are shifted by half a period with respect to the vacuum oscillation, as captured by second-order perturbation theory.

The fact that the system dynamics is characterized by oscillations which do not decay on time scales immediately related to microscopic couplings points to a rather generic and robust cause. We characterize it in terms of the emergence of anomalous spectral properties of the FSS model, which generalize those recently observed [26] in the special case $m = 0$, involving families of special energy eigenstates referred to as “many-body quantum scars”. The latter are constituted by towers of regularly-spaced states in the many-body spectrum with alternating pseudo-momentum $k = 0$ and $k = \pi$, characterized by non-thermal expectation values of local observables as well as by anomalously large overlaps with the charge-density wave initial states. The long-lived coherent oscillating behavior has been attributed in Ref. [26] to the existence of these “scarred” eigenstates.

Figure 5a shows that the modulus of the overlap between the energy eigenstate $|\psi\rangle$ with energy E and the above described inhomogeneous states $|\phi_{q\bar{q}}\rangle$ with momentum k clearly identifies a number of special bands of highly-excited energy eigenstates characterized each by an emerging functional relationship $E(k)$. As shown in Fig. 5d some of the states in these bands strongly deviate from the thermal value $\langle n_j \rangle_{th} \simeq 0.276$. This fact has already been observed in the previously studied quantum-scarred eigenstates, which coincide with the extremal points of these bands at momenta $k = 0$ and $k = \pi$. A closer inspection of these energy-momentum relations, presented in Fig. 5b, shows that they are close to cosine-shaped bands, suggesting the emergence of single-particle excitations in the middle of the many-body energy spectrum.

We further characterize this spectral structure by construct-

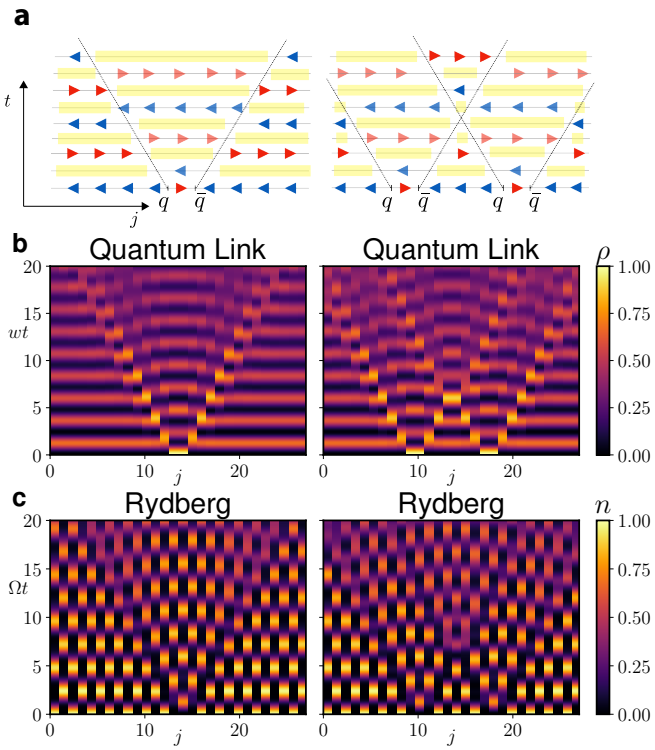


Figure 4: Slow dynamics of particle-antiparticle pairs. **a:** Cartoon states representing the propagation of particle-antiparticle pairs $q-\bar{q}$. The notation is the same as in Fig. 1c, while the yellow stripes denote regions of space with largest particle density and therefore $\langle \hat{E}_{j,j+1} \rangle \simeq 0$. **b:** Evolution of the particle density in the QLM starting from a bare vacuum or "string" state, see Fig. 1c, with initial particle-antiparticle pairs. **c:** Same as in panel b, but in the Rydberg excitation density representation. Left column: the oscillations observed in the light-cone shaped region originating from the particles is expected to be out of phase with respect to those of the bare vacuum. Right column: In the presence of two $q-\bar{q}$ pairs, an additional change of periodicity is expected in correspondence of elastic scattering.

ing a quasi-particle variational ansatz $|\chi_k\rangle$ on top of the exact matrix-product-state zero-energy eigenstate of the Hamiltonian (2) with $\delta = 0$, recently put forward in Ref. [28] (see the supplementary information). As shown in Fig. 5c, the optimal quasi-particle ansatz has the largest overlap with the states on the energy-momentum bands of special eigenstates closest to zero energy, thus reinforcing the above emergent quasi-particle picture.

Discussion

We proved that the large-scale quantum simulation of lattice gauge theories has already been achieved in state-of-the-art experiments with Rydberg atoms, as it can be realized by establishing a mapping between a $U(1)$ gauge theory and Rydberg atom arrays. At the theoretical level, we showed that this novel interpretation provides additional insights into

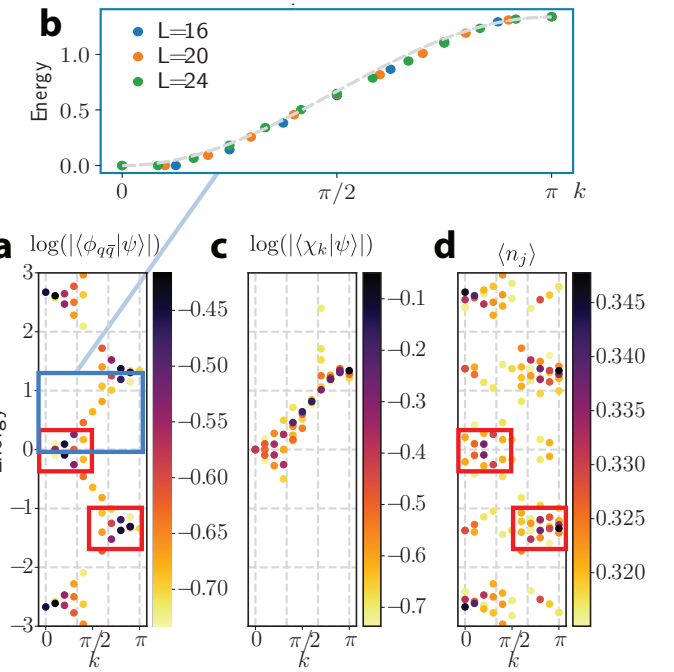


Figure 5: Emergent quasi-particle description of highly-excited states. **a:** Largest overlaps of the initial state $|\phi_{q\bar{q}}\rangle$ with a localized defect in a charge-density wave configuration of the Rydberg-atom chain with the energy eigenstates $|\psi\rangle$ of the FSS Hamiltonian ($\delta = 0, L = 20$) in Eq. (2), as a function of their corresponding momentum and energy. Within the gauge-theory description, the initial state corresponds to having a localized particle-antiparticle pair $q-\bar{q}$. **b:** The eigenstates with the largest overlaps display a regular functional dependence of energy on momentum that is remarkably close to a simple cosine band. **c:** The largest overlaps of the optimal matrix-product state quasi-particle ansatz $|\chi_k\rangle$ built on an exact eigenstate with zero energy (see the main text) accurately reproduce the corresponding emergent quasi-particle band of panel a. **d:** Anomalous (non-thermal) expectation values of a local observable in energy eigenstates. The red boxes highlight the correspondence between the most relevant eigenstates building up $|\phi_{q\bar{q}}\rangle$ (panel a) and the most non-thermal eigenstates (panel d). The emergent spectral structure illustrated in this picture underlies the clean ballistic spreading of particle-antiparticle pairs displayed in Fig. 4.

the exotic dynamics observed in experiments, linking it to archetypal phenomena in particle physics. This immediately implies their generality and applicability to a wide variety of model Hamiltonians within experimental reach. We expect that future studies can further deepen the connection between the statistical mechanics description of such behaviour and its gauge-theoretic interpretation, for instance, elucidating the effects of non-thermal states [26–29] and emergent integrability [30, 31], and the role of confinement in slowing down the dynamics [45–48]. At the experimental level, our findings immediately motivate further experiments along this direction, that can probe different aspects of gauge theories, such as the decay of unstable particle-antiparticle states after a quench, and might be combined with other quantum information protocols [49]. After the present analysis, the experiments per-

formed in Ref. [14] represent a step-stone toward the ambitious realization of non-Abelian gauge theories in three spatial dimension, which remains an outstanding quest [7, 10].

Acknowledgments — We thank M. Aidelsburger, J. Berges, P. Calabrese, M. Collura, A. Dabholkar, P. Hauke, R. Konik, Z. Papic, A. Rudra, and A. Scardicchio for fruitful discussions. MD thanks D. Banerjee, S. Montangero, E. Rico, U.-J. Wiese, and P. Zoller for collaboration on related works, and M. Lukin and H. Pichler for insightful discussions and correspondence. This work is partly supported by the ERC under grant number 758329 (AGEnTh) and by the EU Flagship project Pasquans.

SUPPLEMENTAL MATERIAL

The results presented in this paper are based on exact diagonalization and Krylov-subspace techniques for unitary dynamics. The lattice Schwinger model is conveniently simulated exploiting a mapping to an interacting spin chain [50]. Below, we present the numerical results on the entanglement evolution in the FSS model, and a detailed discussion of the quasi-particle ansatz for the emergent excitations of the spectrum.

Entanglement evolution in the FSS model

We consider the FSS model defined in Eq. (2) of the main text and we investigate the time evolution of the bipartite entanglement entropy $S(t)$ of the chain. We consider as initial state the CDW, which is equivalent to considering the QLM evolving from one of the two uniform string configurations, see Fig. 1 in the main text. In order to determine S , we compute the time-dependent reduced density matrix $\hat{\rho}_R(t)$ of a subsystem consisting of $L/2$ consecutive sites of the chain, by tracing out the degrees of freedom of the remaining complementary $L/2$ sites. In these terms, the von Neumann entanglement entropy is defined by $S(t) = -\text{Tr}[\hat{\rho}_R(t) \ln \hat{\rho}_R(t)]$.

Figures 6a and 6b show the evolution of S for various values of the mass m and of the chain length L , respectively. Information spreading is directly tied to particle production: it is fast at the critical point $m = m_c$ (green curve in Fig. 6a, with $m_c/w = 0.655$, see the main text) or above it $m > m_c$ (red curve), where particles are not confined. For $m < m_c$ (yellow and blue curves), instead, it slows down considerably, as was already observed in the spin-1 QLM [24]. For $m/w = 0$ the change in the original slope of the curve which occurs around $tw \simeq 12$ is due to a finite-volume effect, as demonstrated in Fig. 6b, where such a change progressively disappears upon increasing L . In all cases, the fast oscillations correspond to different stages of pair production.

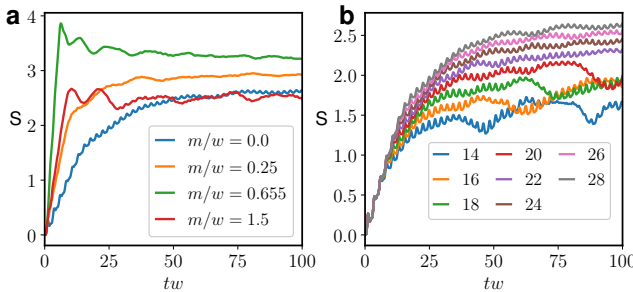


Figure 6: Growth of entanglement entropy in the FSS model. a: Growth of the half-chain entanglement entropy for different values of the particle mass m . Initial state is CDW/string, and $L = 28$. **b:** Growth of entanglement entropy for different sizes L . Initial state is CDW/string, and $m = 0$.

Spectral properties of the FSS model

Robustness of the spectral structure — As shown in the main text, the FSS model for $m = 0$ features the emergence of

regular structures in the middle of the spectrum in terms of energy-momentum bands. We here show that these structures are generically present for sufficiently small values of $|m/w|$. Figure 7 shows the energy-momentum relation of the eigenstates which have largest overlaps with the inhomogeneous state $|\phi_{q\bar{q}}\rangle$ defined in the main text. For $m/w = 0.1$ and $m/w = -0.2$, similar dispersion relations to the case $m/w = 0$ are observed, the main difference being an overall energy shift.

Quasi-particle ansatz for emergent excitations — In order to obtain physical intuition on the emergence of regular energy-momentum bands in highly-excited states which govern the non-equilibrium evolution of localized defects, we propose the following wavefunction

$$|\chi_k\rangle = \sum_{j=1}^L e^{-ikj} \hat{O}_{j-1,j,j+1} |\Phi_{k=0}\rangle, \quad (6)$$

where $|\Phi_{k=0}\rangle$ is the exact eigenstate found in Ref. [28] with momentum $k = 0$ and energy 0, and $\hat{O}_{j-1,j,j+1}$ is a three-site operator depending on a number of variational parameters. Due to the constraints, the space where this operator acts is reduced from dimension 2^3 to 5. The inversion symmetry with respect to site j reduces the number of free variational parameters in $\hat{O}_{j-1,j,j+1}$ to 11. We choose a basis of operators $\{\hat{M}_{j-1,j,j+1}^\alpha\}_{\alpha=1}^{11}$ for parameterizing $\hat{O}_{j-1,j,j+1}$ and define

$$|\phi_k^\alpha\rangle = \sum_{j=1}^L e^{-ikj} \hat{M}_{j-1,j,j+1}^\alpha |\Phi_{k=0}\rangle. \quad (7)$$

For each k , we minimize the energy variance in the space spanned by the states $|\phi_k^\alpha\rangle$. To this aim, we compute the three matrices $N_{\alpha\beta}^k = \langle \phi_k^\alpha | \phi_k^\beta \rangle$, $P_{\alpha\beta}^k = \langle \phi_k^\alpha | \hat{H} | \phi_k^\beta \rangle$, $Q_{\alpha\beta}^k = \langle \phi_k^\alpha | \hat{H}^2 | \phi_k^\beta \rangle$. In order to prevent numerical issues in the minimization, we diagonalize the matrix of the norms N_k and we compute the (rectangular) matrix U^k whose columns are the

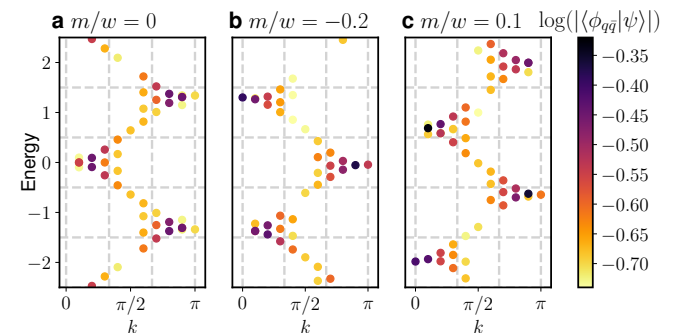


Figure 7: Robustness of the spectral structure. Energy-momentum relation of eigenstates around $E = 0$ for $L = 20$. For each eigenstate $|\psi\rangle$, the colour indicates the value of $\log_{10}(|\langle \psi | \phi_{q\bar{q}} \rangle|)$ (eigenstates with smallest overlaps are not plotted). The dispersion observed for $m/w = 0$ (panel a) is shifted but persists when we introduce a non zero mass (panels b and c).

eigenvectors of N^k having non-zero eigenvalues. We then find the vector $\mathbf{c}_k = (c_k^1, \dots, c_k^m)$ that minimizes

$$\sigma_{\hat{H}}^2 = \frac{\mathbf{c}_k^\dagger U^k Q^k U^k \mathbf{c}_k}{\mathbf{c}_k^\dagger U^k N^k U^k \mathbf{c}_k} - \left(\frac{\mathbf{c}_k^\dagger U^{k\dagger} P^k U^k \mathbf{c}_k}{\mathbf{c}_k^\dagger U^{k\dagger} N^k U^k \mathbf{c}_k} \right)^2. \quad (8)$$

Note that by introducing the matrix U^k we restrict the minimization to states with non-zero norms, thus further reducing the number of variational parameters to $m(k) \leq 11$. The optimal wavefunction is then obtained as

$$|\chi_k\rangle = \sum_{\alpha=1}^{11} \sum_{\beta=1}^m U_{\alpha\beta}^k c_k^\beta |\phi_k^\beta\rangle. \quad (9)$$

Dynamics of the Schwinger model

Simulation of the lattice Schwinger model — The lattice Schwinger model in Eq. (3) of the main text in the gauge-invariant subspace spanned by wavefunctions $|\psi\rangle$ which satisfy the Gauss laws $\hat{G}_j |\psi\rangle = 0$, can be conveniently simulated by exactly mapping it onto an unconstrained chain of spin-1/2 degrees of freedom in the case of open boundary conditions [51]. These spins are obtained from the fermionic operators via a combination of a Jordan-Wigner transformation and a gauge transformation, expressed as

$$\hat{\Phi}_j = \prod_{l=1}^{j-1} \left(\hat{\sigma}_l^z \hat{U}_{l,l+1}^\dagger \right) \hat{\sigma}_j^-. \quad (10)$$

This transformation decouples spins and gauge degrees of freedom, and thus the Hamiltonian (3) in the main text takes the form

$$\hat{H} = -w \sum_{j=1}^{L-1} (\hat{\sigma}_j^+ \hat{\sigma}_{j+1}^- + \text{h.c.}) + \frac{m}{2} \sum_{j=1}^L (-1)^j \hat{\sigma}_j^z + J \sum_{j=1}^{L-1} \hat{E}_{j,j+1}^2. \quad (11)$$

The electric field can be rewritten in terms of the spin operators by means of the Gauss law,

$$\hat{E}_{j,j+1} = \frac{1}{2} \sum_{l=1}^j [\hat{\sigma}_l^z + (-1)^l] - \alpha. \quad (12)$$

Inserting Eq. (12) into Eq. (11) we obtain three additional terms: a long-range spin-spin interaction corresponding to a Coulomb interaction, a local energy offset that modifies the effective mass of the fermions and a linear potential given by the constant background field. The electric field part of the Hamiltonian can be cast in the form:

$$\begin{aligned} \hat{H}_{\text{lat}}^E = & \frac{J}{2} \sum_{n=1}^{L-2} \sum_{l=n+1}^{L-1} (L-l) \hat{\sigma}_n^z \hat{\sigma}_l^z \\ & - \frac{J}{4} \sum_{n=1}^{L-1} [1 - (-1)^n] \sum_{l=1}^n \hat{\sigma}_l^z - J\alpha \sum_{j=1}^{L-1} (L-j) \hat{\sigma}_j^z. \end{aligned} \quad (13)$$

In this form, the non-equilibrium dynamics of the lattice Schwinger model can be efficiently simulated with standard algorithms of quantum many-body physics.

The origin of long-range spin-spin interactions as a consequence of the linear confining Coulomb potential in one spatial dimension is made more evident when Eq. (13) is formulated in terms of the charges $\hat{Q}_j = [\hat{\sigma}_j^z + (-1)^j]/2$ [52]. In the neutral charge sector where $\sum_{j=1}^L \hat{Q}_j = 0$ we have

$$\begin{aligned} \hat{H}_{\text{lat}}^E = & -J \sum_{j=1}^{L-1} \sum_{k=j+1}^L (k-j) \hat{Q}_j \hat{Q}_k \\ & - J \sum_{j=1}^L (L+1-j) \alpha \hat{Q}_j + J \sum_{j=1}^L j \alpha \hat{Q}_j. \end{aligned} \quad (14)$$

The first term describes the Coulomb interaction between charges, while the remaining two terms can be interpreted as interactions with two static charges $-\alpha$ and α , placed at the boundaries of the chain (sites 0 and $L+1$ respectively) and effectively producing the constant background field.

Suppression of string breaking in lattice Schwinger model — The slow relaxation of particle-antiparticle discussed in the main text in the context of the S-1/2 QLM can be immediately generalized to Wilson theories. In Fig. 8, we show that the paradigmatic evolution of a bare string of finite length generated by a particle antiparticle pair in the bare vacuum in the lattice Schwinger model in the absence of background fields ($\theta = 0$) also leads to slow relaxation. One sees that string breaking is strongly suppressed even with moderately weak confinement $J \simeq m, w$ (panels **a**, **b**). Likewise, entanglement entropy growth is also suppressed upon increasing the value of J (panels **c**, **d**).

The massive Schwinger model in the continuum — The massive Schwinger model briefly introduced in the main text describes the quantum electrodynamics of fermions of mass m and charge e in $1+1$ dimensions. Its Lagrangian density is

$$\mathcal{L} = -\frac{1}{4} F_{\mu\nu} F^{\mu\nu} + \bar{\psi} (i\partial^\mu - eA^\mu - m) \psi \quad (15)$$

where $F_{\mu\nu} = \partial_\mu A_\nu - \partial_\nu A_\mu$. The indices $\mu, \nu = 0, 1$ indicate respectively the time and space directions, and the slash notation indicates contraction with the Dirac matrices γ_μ . This model can be formulated in terms of a bosonic field ϕ [43]. We briefly recall here the main points of the derivation of the bosonic Hamiltonian obtained in Ref. [16].

In the Coulomb gauge ($A_1 = 0$), the Euler-Lagrange equation for A_0 yields

$$\partial_1^2 A_0 = -ej_0 \quad (16)$$

where $j_0 = \psi^\dagger \psi$ is the charge density. Integrating Eq. (16), we obtain the continuum version of Eq. (12),

$$F_{01} = -\partial_1 A_0 = e\partial_1^{-1} j_0 + F \quad (17)$$

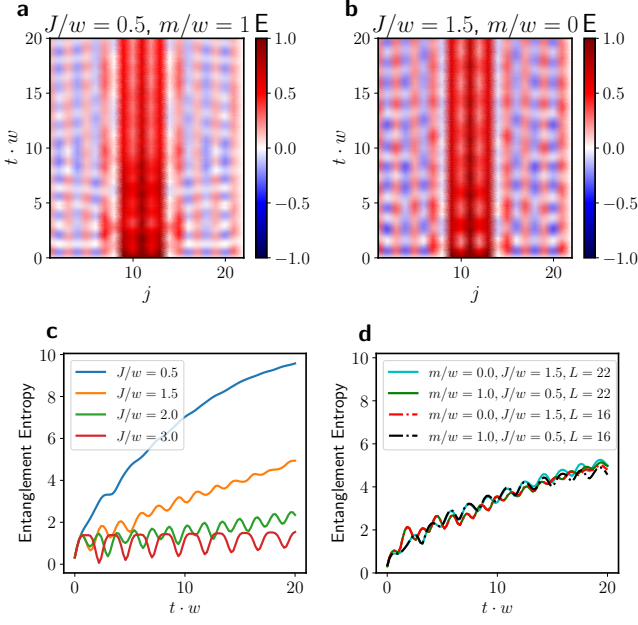


Figure 8: Suppression of string breaking in the lattice Schwinger model. **a, b:** Evolution of the electric flux spatial profile starting from a finite string generated by a particle-antiparticle pair in the bare vacuum. Open boundary conditions are assumed. The plots show that string breaking is strongly suppressed even when the electrostatic energy density is comparable in magnitude with the rest mass and the kinetic energy. **c, d:** Evolution of the half-chain entanglement entropy for the same initial states, in which the bipartition cut is taken in the central bond of the string.

where F is a number, representing a classical background field. The Hamiltonian density obtained from the Lagrangian (15) has the form

$$\mathcal{H} = \bar{\psi}(i\gamma_1\partial_1 + m)\psi + \frac{1}{2}F_{01}^2. \quad (18)$$

The interacting Hamiltonian for the fermions can be formulated using Eq. (17) to integrate out the gauge fields. Integrating by parts in the zero charge sector, i.e., $\int dx j_0(x) = 0$, we obtain

$$H = \int dx \bar{\psi}(i\gamma_1\partial_1 + m)\psi - \frac{e^2}{4} \int dx dy j_0(x)j_0(y)|x - y| - eF \int dx xj_0(x). \quad (19)$$

Similarly to the lattice version of this model [cf. Eqs. (11) and (14)], the resulting Hamiltonian contains the energy of massive free fermions, the Coulomb interaction between charges (which increases linearly in one spatial dimension) and the interactions between the charges and the background field.

The method of bosonization can be applied, by noting that in $1 + 1$ dimensions the conserved vector field $j^\mu = \bar{\psi}\gamma^\mu\psi$ can be written as the curl of a scalar field ϕ

$$j_\mu = \pi^{-1/2}\epsilon_{\mu\nu}\partial^\nu\phi. \quad (20)$$

By substituting in Eq. (17) we get

$$F_{01} = e\pi^{-1/2}\phi + F, \quad (21)$$

and, from the results obtained for a free massive Dirac field [53], we know

$$\bar{\psi}(i\gamma_1\partial_1 + m)\psi \rightarrow N_m \left[\frac{1}{2}\Pi^2 + \frac{1}{2}(\partial_1\phi)^2 + -cm^2 \cos(2\pi^{1/2}\phi) \right]. \quad (22)$$

where $c = e^\gamma/(2\pi)$, $\gamma \simeq 0.577$ is the Euler constant and N_m indicates normal ordering with respect to the mass m . Inserting Eqs. (21) and (22) in Eq. (18), the Hamiltonian density reads

$$\mathcal{H} = N_m \left[\frac{1}{2}\Pi^2 + \frac{1}{2}(\partial_1\phi)^2 - cm^2 \cos(2\pi^{1/2}\phi) + +\frac{e^2}{2\pi} \left(\phi + \frac{\pi^{1/2}F}{e} \right)^2 \right]. \quad (23)$$

By shifting the field $\phi \rightarrow \phi - \pi^{1/2}F/e$ and defining a new normal ordering with respect to the mass $\mu = \pi^{-1/2}e$, we finally obtain

$$\mathcal{H} = N_\mu \left[\frac{1}{2}\Pi^2 + \frac{1}{2}(\partial_1\phi)^2 - cm\mu \cos(2\pi^{1/2}\phi - \theta) + +\frac{\mu^2}{2}\phi^2 \right] \quad (24)$$

where $\theta = 2\pi F/e$. The latter form connects with the discussion in the main text – cf. Eq. (5) therein.

- [1] K. G. Wilson, Phys. Rev. D **10**, 2445 (1974).
- [2] I. Montvay and G. Muenster, *Quantum Fields on a lattice* (Cambridge Univ. Press, Cambridge, 1994).
- [3] Z. Fodor and C. Hoelbling, Rev. Mod. Phys. **84**, 449 (2012).
- [4] K. Fukushima and T. Hatsuda, Rep. Progr. Phys. **74**, 014001 (2010).
- [5] R. Soltz, C. DeTar, F. Karsch, S. Mukherjee, and P. Vranas, Annual Review of Nuclear and Particle Science **65**, 379 (2015).
- [6] E. A. Calzetta and B. L. Hu, *Nonequilibrium Quantum Field Theory* (Cambridge Univ. Press, Cambridge, 2008).
- [7] U. J. Wiese, Ann. Phys. **525**, 777 (2013).
- [8] E. Zohar, I. Cirac, and B. Reznik, Rep. Prog. Phys. **79**, 014401 (2016).
- [9] M. Dalmonte and S. Montangero, Contemp. Phys. **57**, 388 (2016).
- [10] J. Preskill, arXiv.1811.10085 (2018).
- [11] E. A. Martinez, C. A. Muschik, P. Schindler, D. Nigg, A. Erhard, M. Heyl, P. Hauke, M. Dalmonte, T. Monz, P. Zoller, et al., Nature **534**, 516 (2016).
- [12] S. Trotzky, Y.-a. Chen, a. Flesch, I. P. McCulloch, U. Schollwöck, J. Eisert, and I. Bloch, Nat. Phys. **8**, 325 (2012), ISSN 1745-2473.

- [13] I. Bloch, J. Dalibard, and S. Nascimbène, *Nat. Phys.* **8**, 267 (2012).
- [14] H. Bernien, S. Schwartz, A. Keesling, H. Levine, A. Omran, H. Pichler, S. Choi, A. S. Zibrov, M. Endres, M. Greiner, et al., *Nature* **551**, 579 (2017).
- [15] D. Barredo, V. Lienhard, S. de Léséleuc, T. Lahaye, and A. Browaeys, *Nature* **561**, 79 (2018).
- [16] S. Coleman, *Ann. Phys.* **101**, 239 (1976).
- [17] G. S. Bali, H. Neff, T. Düssel, T. Lippert, and K. Schilling (SESAM Collaboration), *Phys. Rev. D* **71**, 114513 (2005).
- [18] F. Hebenstreit, J. Berges, and D. Gelfand, *Phys. Rev. Lett.* **111**, 201601 (2013).
- [19] S. Chandrasekharan and U. J. Wiese, *Nucl. Phys. B* **492**, 455 (1997).
- [20] J. Schwinger, *Phys. Rev.* **128**, 2425 (1962).
- [21] J. Kogut and L. Susskind, *Phys. Rev. D* **11**, 395 (1975).
- [22] F. Hebenstreit, J. Berges, and D. Gelfand, *Phys. Rev. D* **87**, 105006 (2013).
- [23] B. Buyens, J. Haegeman, H. Verschelde, F. Verstraete, and K. Van Acoleyen, *Phys. Rev. X* **6**, 041040 (2016).
- [24] T. Pichler, M. Dalmonte, E. Rico, P. Zoller, and S. Montangero, *Phys. Rev. X* **6**, 011023 (2016).
- [25] K. Rajagopal and F. Wilczek, *Nucl. Phys. B* **404**, 577 (1993).
- [26] C. Turner, A. Michailidis, D. Abanin, M. Serbyn, and Z. Papić, *Nature Physics* **14**, 745 (2018).
- [27] C. J. Turner, A. A. Michailidis, D. A. Abanin, M. Serbyn, and Z. Papić, *Phys. Rev. B* **98**, 155134 (2018).
- [28] C.-J. Lin and O. I. Motrunich, arXiv preprint arXiv:1810.00888 (2018).
- [29] W. W. Ho, S. Choi, H. Pichler, and M. D. Lukin, *Phys. Rev. Lett.* **122**, 040603 (2019).
- [30] S. Choi, C. J. Turner, H. Pichler, W. W. Ho, A. A. Michailidis, Z. Papić, M. Serbyn, M. D. Lukin, and D. A. Abanin, arXiv preprint arXiv:1812.05561 (2018).
- [31] V. Khemani, C. R. Laumann, and A. Chandran, arXiv preprint arXiv:1807.02108 (2018).
- [32] I. Lesanovsky and H. Katsura, *Phys. Rev. A* **86**, 041601 (2012).
- [33] J. Zeiher, J. yoon Choi, A. Rubio-Abadal, T. Pohl, R. van Bijnen, I. Bloch, and C. Gross, *Phys. Rev. X* **7**, 041063 (2017).
- [34] P. Fendley, K. Sengupta, and S. Sachdev, *Phys. Rev. B* **69**, 075106 (2004).
- [35] S. Chandrasekharan and U.-J. Wiese, *Nucl. Phys. B* **492**, 455 (1997).
- [36] D. Horn, *Phys. Lett. B* **100**, 149 (1981).
- [37] D. Banerjee, M. Dalmonte, M. Müller, E. Rico, P. Stebler, U.-J. Wiese, and P. Zoller, *Phys. Rev. Lett.* **109**, 1 (2012).
- [38] B. M. McCoy and M.-L. Yan, *Nucl. Phys. B* **215**, 278 (1983).
- [39] N. Chepiga and F. Mila, arXiv preprint arxiv.1809.00746 (2018).
- [40] Y.-P. Huang, D. Banerjee, and M. Heyl, arXiv preprint arXiv:1808.07874 (2018).
- [41] V. Kasper, F. Hebenstreit, M. Oberthaler, and J. Berges, *Phys. Lett. B* **760**, 742 (2016).
- [42] E. Rico, T. Pichler, M. Dalmonte, P. Zoller, and S. Montangero, *Phys. Rev. Lett.* **112**, 201601 (2014).
- [43] C. J. Hamer, J. Kogut, D. P. Crewther, and M. M. Mazzolini, *Nucl. Phys. B* **208**, 413 (1982).
- [44] M. Bañuls, K. Cichy, I. Cirac, and K. Jansen, *J. High Energy Phys.* **2013**, 158 (2013).
- [45] M. Kormos, M. Collura, G. Takács, and P. Calabrese, *Nature Physics* **13**, 246 (2017).
- [46] M. Brenes, M. Dalmonte, M. Heyl, and A. Scardicchio, *Phys. Rev. Lett.* **120**, 030601 (2018).
- [47] P. P. Mazza, G. Perfetto, A. Lerose, M. Collura, and A. Gambassi, arXiv pre-prints arXiv:1806.09674 (2018).
- [48] A. J. A. James, R. M. Konik, and N. J. Robinson, arXiv pre-prints arXiv:1804.09990 (2018).
- [49] C. Kokail, C. Maier, R. van Bijnen, T. Brydges, M. K. Joshi, P. Jurcevic, C. A. Muschik, P. Silvi, R. Blatt, C. F. Roos, et al., arXiv:1810.03421 (2018).
- [50] C. J. Hamer, Z. Weihong, and J. Oitmaa, *Phys. Rev. D* **56**, 55 (1997).
- [51] T. Banks, L. Susskind, and J. Kogut, *Phys. Rev. D* **13**, 1043 (1976).
- [52] P. Sala, T. Shi, S. Kühn, M. C. Bañuls, E. Demler, and J. I. Cirac, *Phys. Rev. D* **98**, 034505 (2018).
- [53] S. Coleman, *Phys. Rev. D* **11**, 2088 (1975).